Supplementary Table 1. Crystallographic statistics

	Native	Se-Met	$Ta_6Br_{12}^{2+}$	K_2PtBr_4	C_2H_5HgCl
Data collection	NSLS X29	NSLS X29	NSLS X29	NSLS X29	NSLS X25
Wavelength (Å)	1.0750	0.9768	1.2547	1.0716	1.0057
Space group	$C222_1$	$C222_1$	$C222_1$	$C222_1$	$C222_1$
Cell dimensions (Å)	101.7, 307.1, 187.6	100.6, 305.4, 188.5	101.8, 306.8, 187.8	101.5, 307.2, 189.5	103.1, 304.4, 188.4
Resolution (Å)	30 - 3.4	35 - 7.5	30 - 4.5	50 - 6.5	30 - 7.2
R_{sym} (%)	7.8 (50.6)	7.4 (39.7)	5.0 (49.4)	4.5 (43.3)	5.1 (33.1)
I / σI	17.4 (1.9)	11.0 (4.0)	13.0 (1.8)	19.3 (4.6)	18.0 (5.6)
Completeness (%)	97.4 (81.8)	99.9 (100.0)	98.9 (90.9)	98.7 (99.4)	100.0 (100.0)
Redundancy	9.4 (5.2)	4.7 (4.7)	4.6 (3.6)	5.1 (5.1)	5.0 (5.2)
Sites found		7	12	17	12
Mean Figure of Merit	0.64				
Refinement				$KAu(CN)_2$	$(C_2H_5HgO)HPO_2$
Resolution (Å)	20 - 3.4		**Data collection**	APS 24-ID-E	APS 24-ID-E
No. reflections	33,422		Wavelength (Å)	0.9792	0.9792
R_{work} / R_{free} (%)	21.6 / 26.1		Space group	$C222_1$	$C222_1$
No. atoms	11,548		Cell dimensions (Å)	101.6, 307.2, 187.1	102.0, 308.3, 189.0
Average B-factors (Å^2)	180.0		Resolution (Å)	30 - 7.0	40 - 7.8
R.m.s deviations			R_{sym} (%)	7.1 (45.8)	9.6 (43.8)
Bond lengths / angles	0.012 Å / 1.59 °		I / σI	10.1 (2.5)	7.7 (2.3)
Ramachandran plot			Completeness (%)	99.6 (99.9)	99.8 (100.0)
Most favored / allowed	69.9 % / 99.6 %		Redundancy	3.9 (4.0)	4.9 (5.1)
			Sites found	14	8

†Highest resolution shell is shown in parenthesis.

Supplementary Table 2. Number of observed Se-sites in the anomalous difference Fourier

Se-site	Predict*	M^1	M^2	M^3	M^4	M^5	M^6	$I4^1$	$I4^2$	$I4^3$	$I4^4$	$I2^1$	$I2^2$	$I2^3$	$I2^4$
MyD88	2	1	1	2	2	2	2	0	-	-	-	-	-	-	-
IRAK4	0	-	-	-	-	-	-	0	0	0	0	0	-	-	-
IRAK2	4	-	-	-	-	-	-	-	-	-	-	4	4	4	3

*The first Met residues were excluded.

Supplementary Table 3. Pairwise superposition among MyD88 DD, IRAK4 DD and IRAK2 DD, with PIDD DD and RAIDD DD, and with the isolated IRAK4 DD

	IRAK4	IRAK2	PIDD	RAIDD	IRAK4 (2a9i)*
MyD88	77 Cα, 1.22 Å	74 Cα, 1.29 Å	62 Cα, 1.60 Å	56 Cα, 1.46 Å	
IRAK4		82 Cα, 1.16Å	52 Cα, 1.49 Å	59 Cα, 1.52 Å	105 Cα, 0.70 Å
IRAK2			54 Cα, 1.52 Å	53 Cα, 1.57 Å	

*Structure of IRAK4 DD in isolation.

Supplementary Table 4. Structural homology search using the DALI server*

	Top match			Second match		
	Name	PDB	Z-score	Name	PDB	Z-score
MyD88	UNC5H2	1wmg	11.4	IRAK4	2a9i	11.2
IRAK4	Tube	1d2z	13.8	Pelle	1d2z	12.9
IRAK2	Pelle	1d2z	13.6	IRAK4	2a9i	12.7

*Holm, L. and Sander, C., Dali: a network tool for protein structure comparison. *Trends Biochem. Sci.* **20**, 478 (1995).

Supplementary Figure 1. The gel filtration profile and the MALS measurement of the MyD88: IRAK4 DD complex. The calculated molecular mass for 6: 4, 7: 4 or 8: 4 stoichiometry of the MyD88: IRAK4 complex is shown. A molecular mass of 135.4 kDa (0.5% error) was obtained, which could best represent a 7:4 stoichiometry with a calculated molecular mass of 139.1 kDa. However, it is most likely that the gel filtration peak contains complexes of variable stoichiometry with an average molecular mass of ~135 kDa, including the major species of 7: 4 and 8: 4 complexes and the 6: 4 complex observed under a mild stripping mass spectrometry condition (Motshwene, P. G. et al., An oligomeric signaling platform formed by the Toll-like receptor signal transducers MyD88 and IRAK-4. J Biol Chem 284 (37), 25404 (2009)). In the crystal, both 7: 4 and 8: 4 complexes can be accommodated without causing steric hindrance in crystal packing. No additional MyD88 molecules were observed probably due to their lower occupancies in the crystal. The SDS-PAGE shows the two gel filtration peaks; upper band is IRAK4 and the lower band is MyD88.

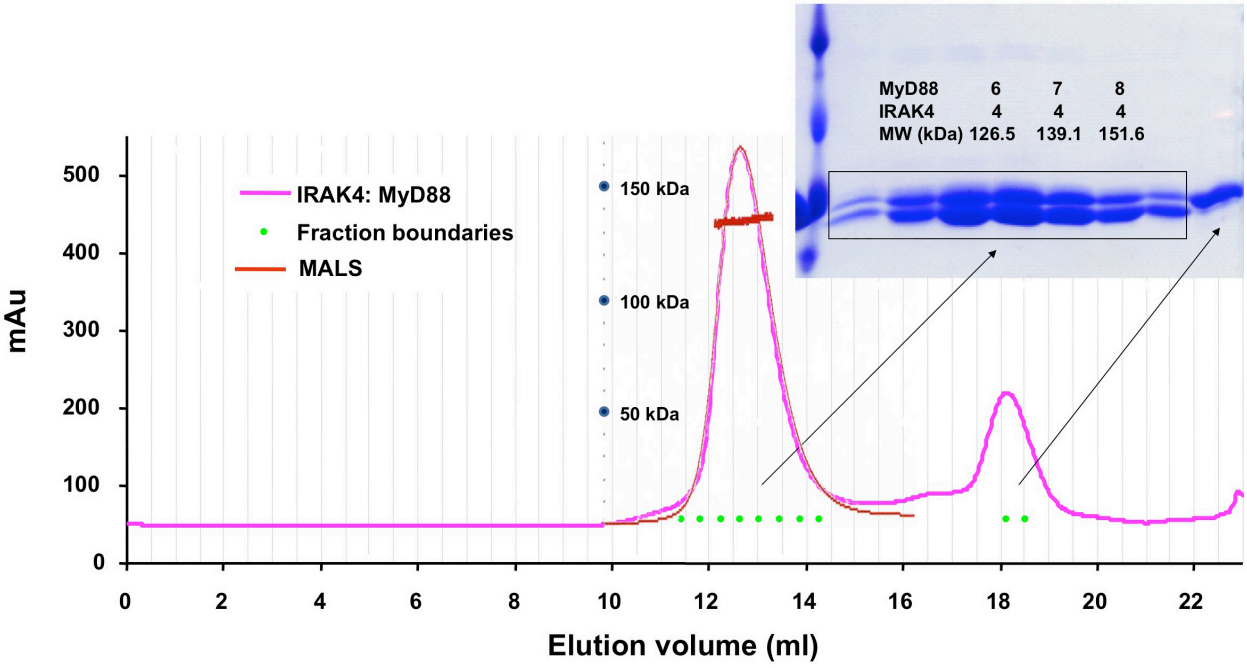

Supplementary Figure 2. Experimental electron density map superimposed with the final atomic model

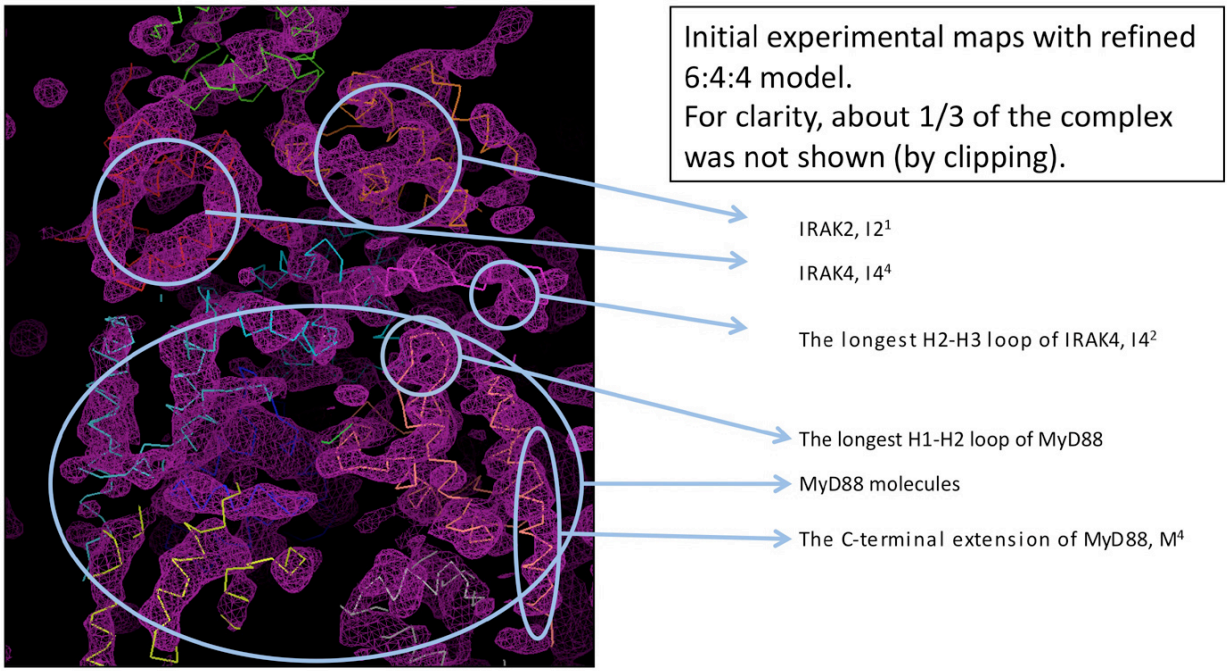

Supplementary Figure 3. SDS-PAGE of the MyD88: IRAK4 binary and the MyD88: IRAK4: IRAK2 ternary complexes

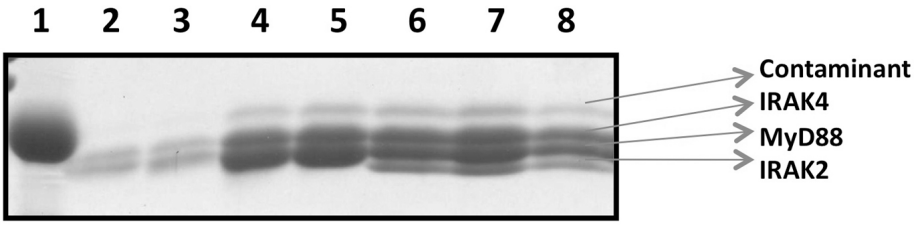

1. LMW marker of 14kDa.
2. MyD88: IRAK4 complex (diluted)
3. MyD88: IRAK4 complex (diluted, different fractions)
4. MyD88: IRAK4 complex
5. MyD88: IRAK4 complex (different fractions)
6. MyD88: IRAK4: IRAK2 complex
7. MyD88: IRAK4: IRAK2 complex (different fractions)
8. MyD88: IRAK4: IRAK2 complex (different fractions)

Supplementary Figure 4. Surface diagrams of each of the layers. The size of the central cavity in the MyD88 layers has an estimated diameter of ~15 Å at the widest part and a depth of ~35 Å.

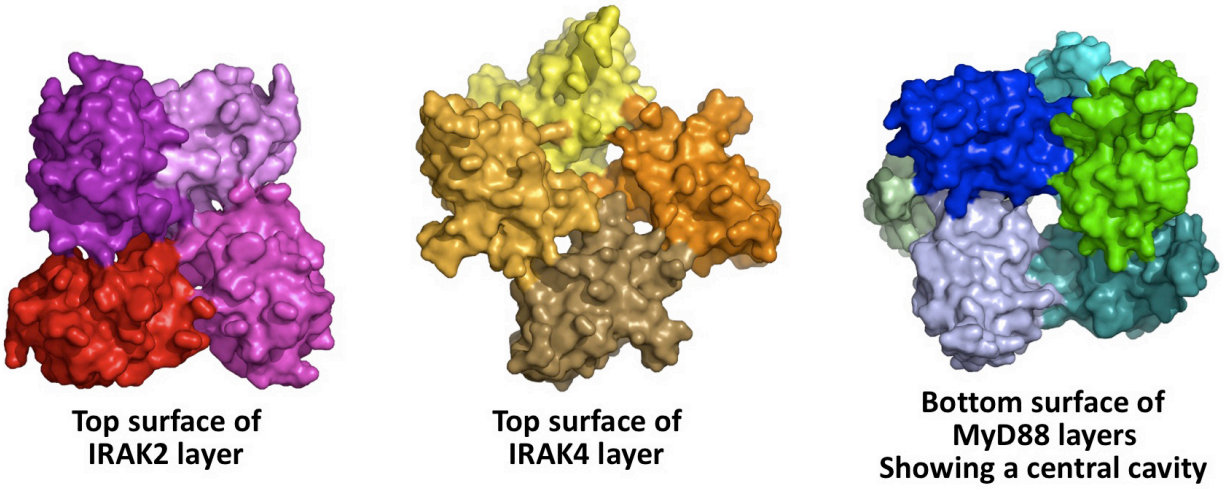

Supplementary Figure 5. Two human disease mutations of MyD88, ΔE52 and L93P, map to the H2 and H5 helices of the DD, respectively. The ΔE52 mutation would have changed the register of residues on the helix and disrupt the folding. Because L93 side chain is buried, the L93P mutation will not only affect the helix formation but also hydrophobic core of the DD.

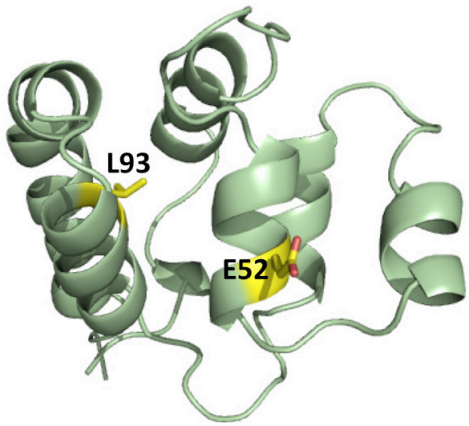

Supplementary Figure 6. Temperature factor distribution in the ternary complex using rainbow colors with low temperature factors in the blue end and high temperature factors in the red end of the spectrum.

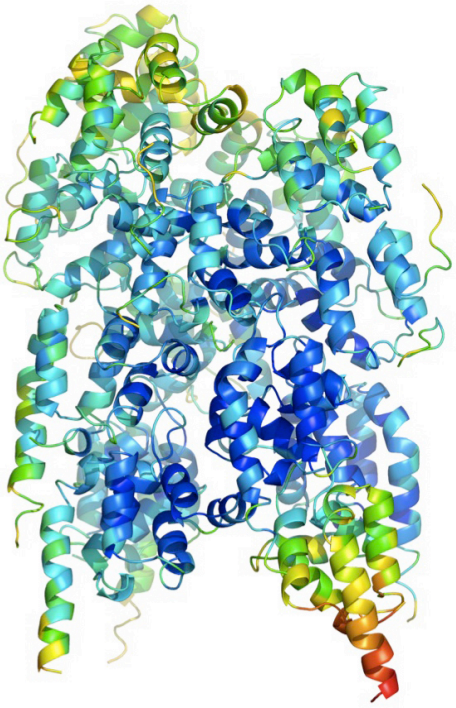

Supplementary Figure 7. Detailed interactions in the ternary complex. Buried surface areas and shape complementarity (sc) scores are shown. Side chains are labeled. Molecules are shown in the same color coding as in Fig. 1a. a, A schematic diagram showing the three types of interactions in the complex. b, The three type I interactions in the complex, MyD88: MyD88, MyD88: IRAK4 and IRAK4: IRAK2. c, The three type II interactions in the complex, MyD88: MyD88, MyD88: IRAK4 and IRAK4: IRAK2. d, The five type III interactions in the complex, MyD88: MyD88, MyD88: IRAK4, IRAK4: IRAK4, IRAK4: IRAK2 and IRAK2: IRAK2.

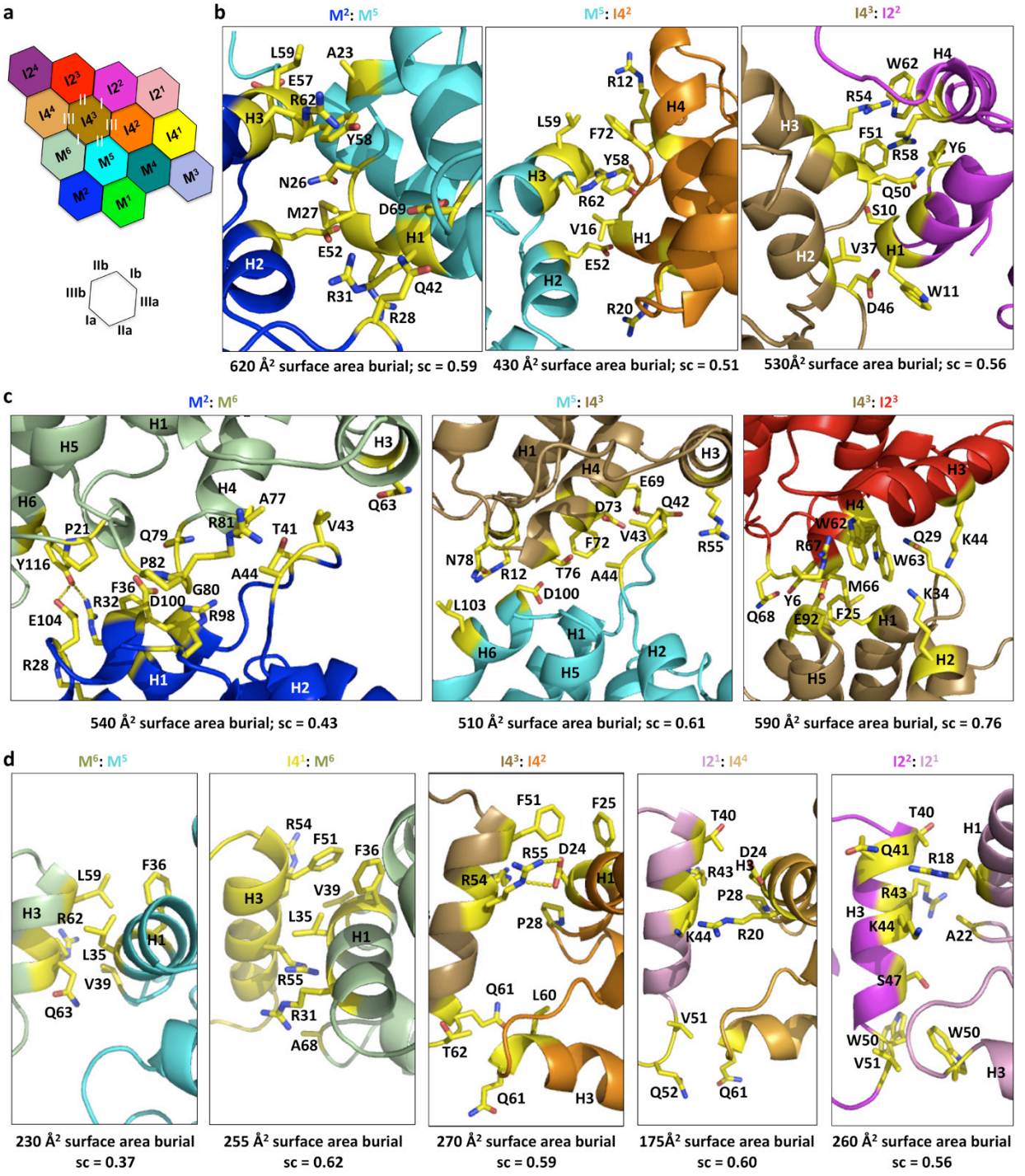

Supplementary Figure 8. Superpositions of the three type I interactions, the three type II interactions and the five type III interactions in the ternary complex. Ribbon diagrams of the superpositions are shown at the top panel. The RMSDs and the number of superimposed Cα atoms are shown at the lower panel. For comparison, the RMSDs and the number of superimposed Cα atoms are also shown for the PIDD: RAIDD complex.

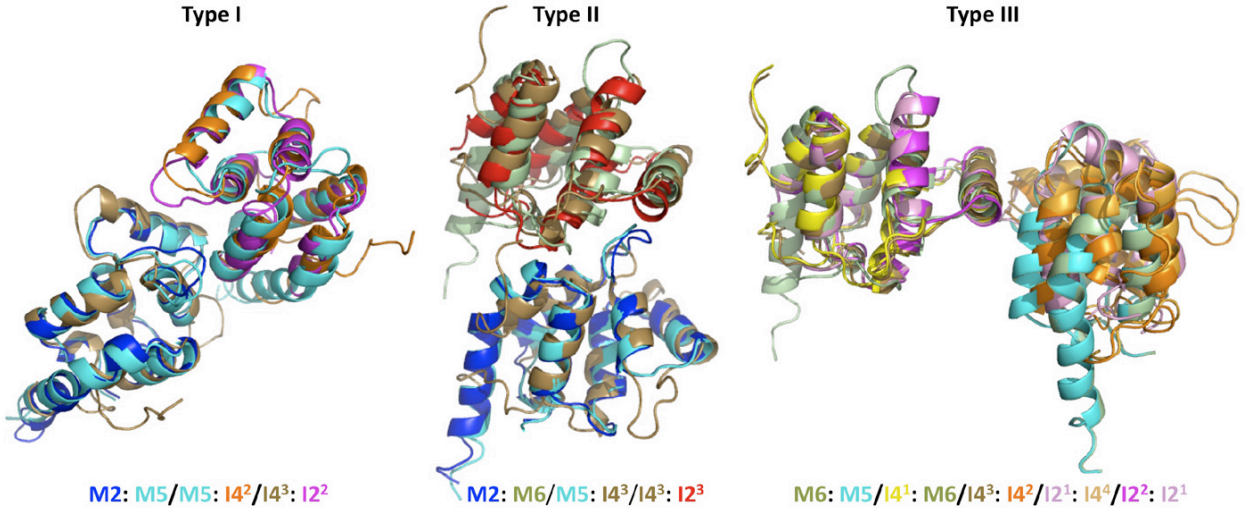

MyD88:IRAK4:IRAK2											
Surface type	I			II			III				
Pairs	M2:M5	M5:I4^2	I4^3:I2^2	M2:M6	M5:I4^3	I4^3:I2^3	M6:M5	I4^1:M6	I4^3:I4^2	I2^1:I4^4	I2^2:I2^1
RMSD (Å)	Ref	1.4	1.8	Ref	1.4	1.9	Ref	1.1	1.7	2.1	2.3
# Atoms		183	162		181	162		181	157	163	164
RMSD (Å)		Ref	1.6		Ref	1.6		Ref	1.1	1.5	1.9
# Atoms			166			167			183	162	171
RMSD (Å)									Ref	0.9	1.4
# Atoms										192	171
RMSD (Å)										Ref	0.9
# Atoms											178
PIDD:RAIDD											
Surface type	I			II			III				
Pairs	P5:P1	P1:R2	R5:R1	R1:P1	R6:R5		P1:P2	R5:P1	R4:R5		
RMSD (Å)	Ref	1.6	2.0	Ref	1.7		Ref	1.3	2.4		
# Atoms		178	161		170			166	160		
RMSD (Å)		Ref	1.4					Ref	1.6		
# Atoms			166						170		

Ref: reference molecule

Supplementary Figure 9. Residues critical for ternary complex formation. a, Structure-based alignment of all sequences except that IRAK1 and dMyD88 sequences were aligned by matching the highly conserved residues of all sequences. Residues with buried surface areas larger than 50 Å^2 are colored according to their locations on type Ia, Ib, IIa, IIb, IIIa, or IIIb surfaces. Only one residue, which is in IRAK2, has a surface area burial larger than 50 Å^2 and is shaded in gray. Mutagenesis sites are marked with the resulting changes below the sequences. Mutations or double mutations that caused significant effects are colored or underlined in red, respectively. Mutations that did not express are colored in black. Other mutations are colored in cyan. Tube and dMyD88 mutations are from a previous study (Sun, H. et al., Regulated assembly of the Toll signaling complex drives Drosophila dorsoventral patterning. Embo J 23 (1), 100 (2004)). Approximate locations of H1 to H6 are shown based on the average positions of helices in the DD structures. The long H6 in MyD88 is a combination of the labeled H6 and the Extension. b, Pulldown of WT MyD88-long (residues 20-154) by His-tagged WT and mutant IRAK4 at its MyD88-interacting interfaces. c, Pulldown of WT IRAK4 DD by His-tagged WT and mutant MyD88 DD at its IRAK4-interacting surfaces. d, Pulldown of WT MyD88-long and IRAK4 by His-tagged WT and mutant IRAK2 at its IRAK4-interacting surfaces. e, Pulldown of diubiquitin fusion of WT IRAK2 and MyD88-long by His-tagged WT and mutant IRAK4 at its IRAK2-interacting interfaces. *: contaminant.

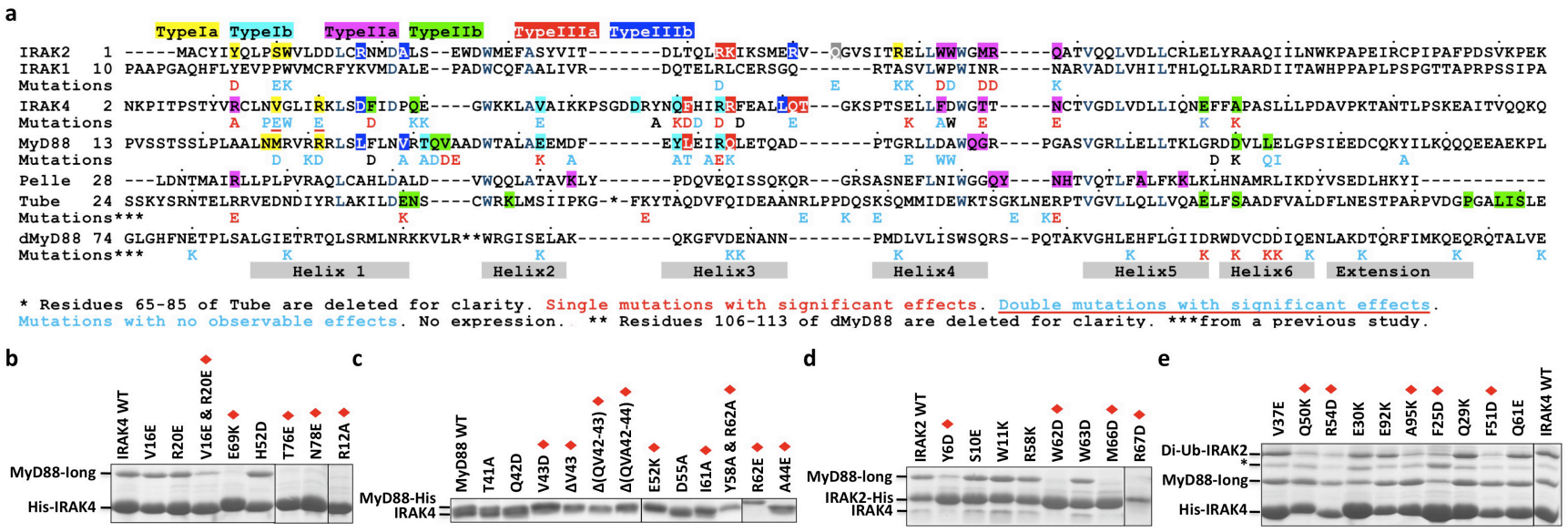

Supplementary Figure 10. Pairwise co-expression experiments among MyD88, IRAK1, IRAK2 and IRAK4

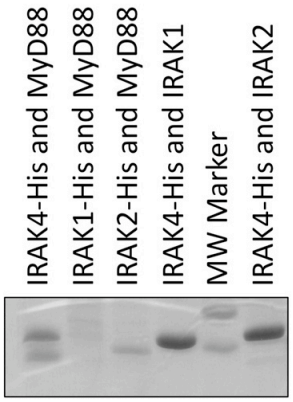

Supplementary Figure 11. Relationship between double-stranded helical symmetry and single-stranded helical symmetry in a schematic diagram. The 5 PIDD (P): 7 RAIDD (R) complex is used as an example. In the left panel, the interaction surfaces of adjacent DDs in the first and second helical strands are labeled with red and blue lines, respectively. These red or blue lines should align at the same height along the helical axis. In the right panel, the adjacent DDs in the single helical strand are labeled with red lines of the same widths. In the left panel, the two adjacent DDs skip a "notch" so that two helices co-exist in the complex. The two helices are P^1, P^2, P^3, R^1, R^2, R^3 and $P^{1'}$, $P^{2'}$, $R^{1'}$, $R^{2'}$, $R^{3'}$, $R^{4'}$. In the right panel, the assembly is rotated to the left to become less steep along the helical axis so that P^3 is connected to $P^{1'}$ in a single helical symmetry. The single helix would have the order of P^1, P^2, P^3, $P^{1'}$, $P^{2'}$, $R^{1'}$, $R^{2'}$, $R^{3'}$, R^1, R^2, R^3, $R^{4'}$.

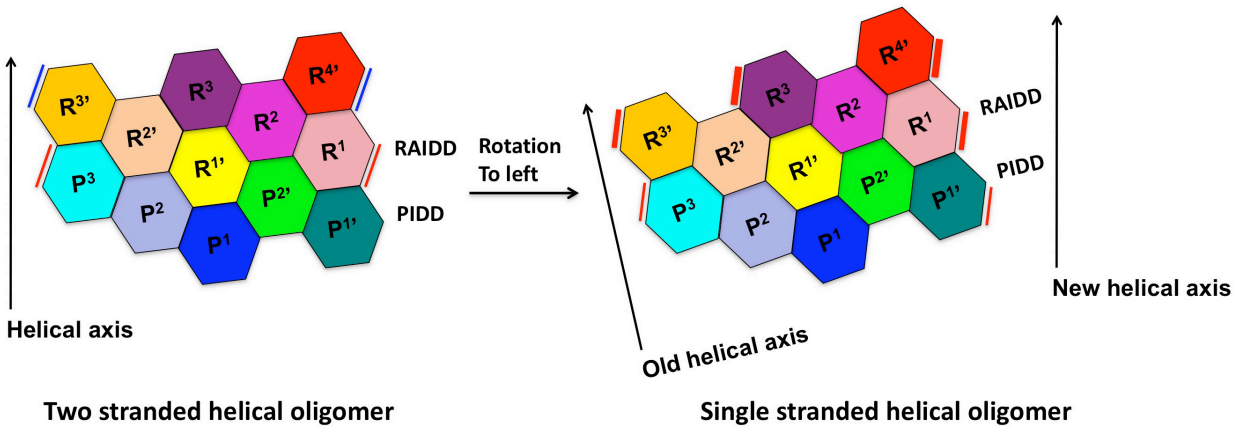

Supplementary Discussion 1. Stoichiometry of the complex in solution and in the crystal

Previous nano-electrospray ionization mass spectra of a MyD88: IRAK4 DD complex acquired under conditions that preserve non-covalent interactions showed a major species with a stoichiometry of 7:4 and a second species with a stoichiometry of 8:4 [1]. At higher activation energies, stoichiometries of 6:4, 7:3, and 8:3 "stripped complexes" after ejection of single subunits were observed following gas phase dissociation events [1]. Our multi-angle light scattering (MALS) measurement of the MyD88: IRAK4 complex gave a molecular mass of 135.4 kDa (0.5% error) (Supplementary Fig. 1), which could best represent a 7:4 stoichiometry with a calculated molecular mass of 139.1 kDa. However, it is most likely that the complex contains populations of variable stoichiometries with an average molecular mass of ~135 kDa, possibly including but not limited to 7:4, 8:4 and 6:4 complexes. On a molecular level, this variable stoichiometry of MyD88 may be contributed by its uniquely long H1-H2 loop, which inserts between two adjacent MyD88 molecules, making MyD88 self-assembly possible. In the crystal, both 7:4 and 8:4 complexes with one and two additional MyD88 molecules, respectively, can be accommodated without causing steric hindrance in crystal packing. No additional MyD88 molecules were observed probably due to their lower occupancies in the crystal.

1 Motshwene, P. G. et al., An oligomeric signaling platform formed by the Toll-like receptor signal transducers MyD88 and IRAK-4. *J Biol Chem* **284** (37), 25404 (2009).

Supplementary Discussion 2. Cooperativity in the assembly of the complex

Assembly of the MyD88: IRAK4 and the MyD88: IRAK4: IRAK2 complexes should both be highly cooperative given the involvement of multiple subunits in the process. This cooperativity implies that formation of the complex has a steep dependence on receptor-mediated clustering of MyD88 and on concentrations of the component proteins in the cell. This high dependence ensures that assembly of the complex and induction of signaling are tightly regulated.